JACS
JOURNAL OF THE AMERICAN CHEMICAL SOCIETY

Article

pubs.acs.org/JACS

Metallic Conductivity in a Two-Dimensional Cobalt Dithiolene Metal–Organic Framework

Andrew J. Clough,[‡] Jonathan M. Skelton,[§] Courtney A. Downes,[‡] Ashley A. de la Rosa,[‡] Joseph W. Yoo,[‡] Aron Walsh,[†] Brent C. Melot,*[,‡] and Smaranda C. Marinescu*[,‡]

[‡]Department of Chemistry, University of Southern California (USC), Los Angeles, California 90089, United States
[§]Department of Chemistry, University of Bath, Bath BA2 7AY, United Kingdom
[†]Department of Materials, Imperial College London, London SW7 2AZ, United Kingdom

Supporting Information

ABSTRACT: Two-dimensional (2D) metal–organic frameworks (MOFs) have received a great deal of attention due to their relatively high charge carrier mobility and low resistivity. Here we report on the temperature-dependent charge transport properties of a 2D cobalt 2,3,6,7,10,11-triphenylenehexathiolate framework. Variable temperature resistivity studies reveal a transition from a semiconducting to a metallic phase with decreasing temperature, which is unprecedented in MOFs. We find this transition to be highly dependent on the film thickness and the amount of solvent trapped in the pores, with density functional theory calculations of the electronic-structure supporting the complex metallic conductivity of the material. These results identify the first experimentally observed MOF that exhibits band-like metallic conductivity.

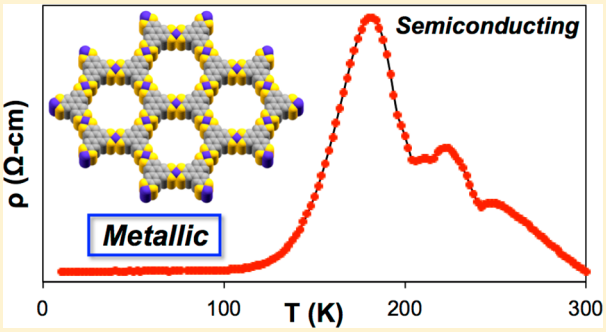

INTRODUCTION

The development of inexpensive yet highly efficient catalysts for solar-to-fuel energy conversion is vital for mitigating the adverse effects that hydrocarbon fuels have on the environment.[1] Immobilization of molecular catalytic units is an attractive strategy for bridging the gap between homogeneous and heterogeneous electrocatalysis for solar-to-fuel applications.[2] This approach retains the desirable properties of molecular systems, like well-defined chemistries and clear design principles, while also taking advantage of the robust efficiency of heterogeneous catalysts.[2] Metal–organic frameworks, a rapidly expanding class of nanoporous coordination polymers,[3] have attracted growing attention because they sit at the interface between molecules and extended solids, offering a mixture of high surface area-to-volume ratio and site-isolation of catalytic units, all of which are indicators to systems with enhanced activities. Yet, the biggest challenge these materials face for designing new electrocatalysts is rooted in their ability to efficiently transport charge between the metals and their coordinating ligands.[4]

In this regard, 2D frameworks[5] have been shown to exhibit high charge-carrier mobility because of in-plane charge delocalization and extended π-conjugation within the sheets.[6] Recent studies have demonstrated that nickel or copper 2,3,6,7,10,11-hexaiminotriphenylene ($M_3(HITP)_2$, M = Ni, Cu) frameworks exhibit thin film conductivities on the order of 40 $S \cdot cm^{-1}$, whereas copper benzenehexathiolate shows conductivities up to 1580 $S \cdot cm^{-1}$, which is the highest conductivity reported for a coordination polymer.[7] Yet, the transport properties are usually the result of inadvertent doping of an intrinsic semiconductor that can be synthetically difficult to control rather than a truly metallic charge delocalization.

In a previous report, we showed that 2,3,6,7,10,11-triphenylenehexathiolate can be used to produce a periodic 2D network of cobalt dithiolene units as illustrated in Figure 1.[8] This phase displays remarkable activity for the electrocatalytic H_2 evolution from water,[8] and is one of the first examples of an electrocatalytically active MOF.[9] This motivated us to investigate the source of this high catalytic performance by characterizing its charge transport characteristics. Here, we report the first observation of a temperature-dependent transition in a MOF from a semiconducting to a metallic phase with decreasing temperature using a combination of thin film resistivity measurements and density functional theory (DFT) calculations, with metallic conductivity persisting to temperatures as high as 225 K.

RESULTS AND DISCUSSION

Framework **1** was prepared using a slightly modified procedure from previous reports.[8] The material adopts a hexagonal 2D structure with long-range order in the *ab* plane as evidenced by the sharp Bragg reflections in the synchrotron X-ray diffraction pattern shown in Figure 2. The pattern exhibits prominent peaks

Received: June 2, 2017
Published: July 13, 2017

DOI: 10.1021/jacs.7b05742
J. Am. Chem. Soc. 2017, 139, 10863–10867

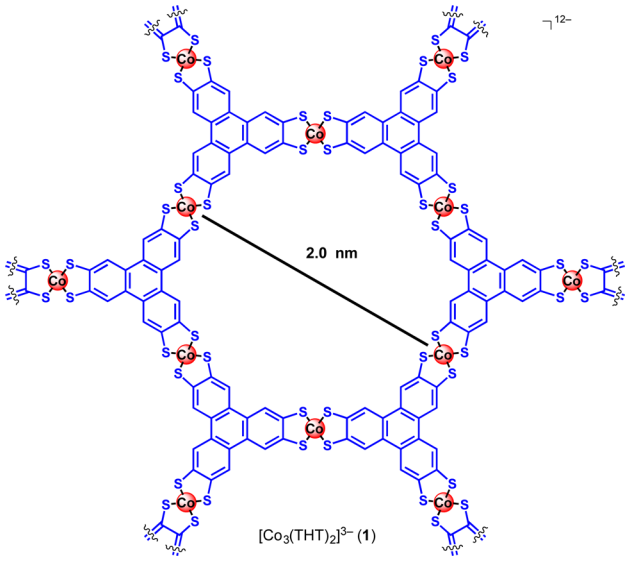

Figure 1. Structure of the 2D cobalt dithiolene framework $[Co_3(THT)_2]^{3-}$, **1**, studied here.

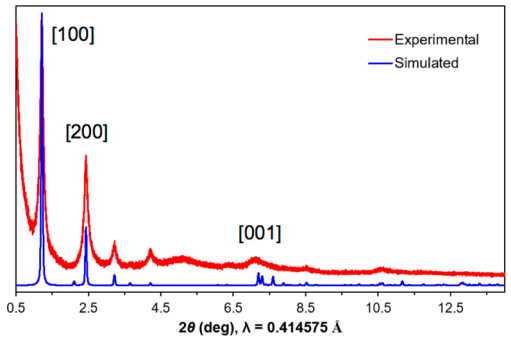

Figure 2. Experimental and simulated PXRD patterns of **1**.

at 1.2°, 2.4°, 3.2°, and 4.2°, which correspond to a significant degree of coherence within the 2D sheets. The somewhat broader reflection at 7.2° corresponds to the [001] reflection, suggesting less coherence between the sheets as is common for layered materials.[10] Regardless, the experimental diffraction pattern is a close approximation to simulations from the Materials Studio suite of programs (Figure S1) using the idealized structure with layers that are stacked in perfect registry. The optimized structure is best described using P6/*mmm* as the space group with unit cell parameters of $a = b = 22.52$ Å and $c = 3.3$ Å (Figure 2).

Gas sorption isotherms performed on **1** reveal a Brunauer–Emmett–Teller (BET) surface area of 370 $m^2\ g^{-1}$ (Figure S3), which is similar to that of the previously reported platinum analogue.[6f] Temperature-dependent susceptibility measurements show a response characteristic of localized moments. A fit of the high temperature magnetic susceptibility data (200–300 K) to the Curie–Weiss equation ($\chi = C/(T - \theta_{CW}) + \chi_0$) yields an effective paramagnetic moment, $\mu_{eff} = 1.55\ \mu_B$ per formula unit, $\theta_{CW} = -34$ K, and $\chi_0 = 3.57 \times 10^{-4}$ emu mol^{-1} Oe^{-1} (Figure S4). The positive temperature-independent term reflects a background paramagnetic signal that could result from the presence of some charge delocalization or more simply from second-order Zeeman effects.[11] The moment is slightly reduced from what is expected for an S = 1/2 state, which should show a theoretical moment of 1.87 μ_B. Such an underestimate is often ascribed to orbital quenching due to covalency, and indicates the presence of only one unpaired spin per formula unit. Given the presence of three square-planar cobalt ions per unit cell, this is consistent with two-thirds of the Co adopting the trivalent state (S = 0) with one exhibiting a formal divalent (S = 1/2) state, which is significant because mixed oxidation states are often associated with charge delocalization.[12]

The temperature-dependent resistivity of **1** was measured using a four-point Van der Pauw geometry on a pressed pellet of **1** with a thickness of 0.24(2) mm. Graphitic carbon paint (Alfa Aesar) was used to create Ohmic contacts, as verified by the linear I-V trace shown in Figure S5. InGa eutectic and silver paint were also used to create Ohmic contacts and gave qualitatively similar results; however, the carbon paint was the best at maintaining physical contact over the entire temperature range of interest. At 300 K, the bulk resistivity was determined to be 0.720(7) kΩ·cm, corresponding to a conductivity of 1.4×10^{-3} S·cm^{-1}, which is in line with values reported for the platinum analogue.[6f] Given the highly anisotropic nature of the pressed pellet of **1**, this relatively low value is likely associated with the random orientation of the powder and is exaggerated by grain-boundary scattering between the sheet-like particles.

An exponential rise in the resistivity of the pellet is seen between 300 and 170 K, as would be expected for a semiconducting sample where transport is dominated by thermally populated carriers that must overcome a hopping barrier for conduction (Figure 3a).[13] An Arrhenius fit to the data suggests an activation energy on the order of 173 meV (Figure S6). More interestingly, a decrease in the resistivity is

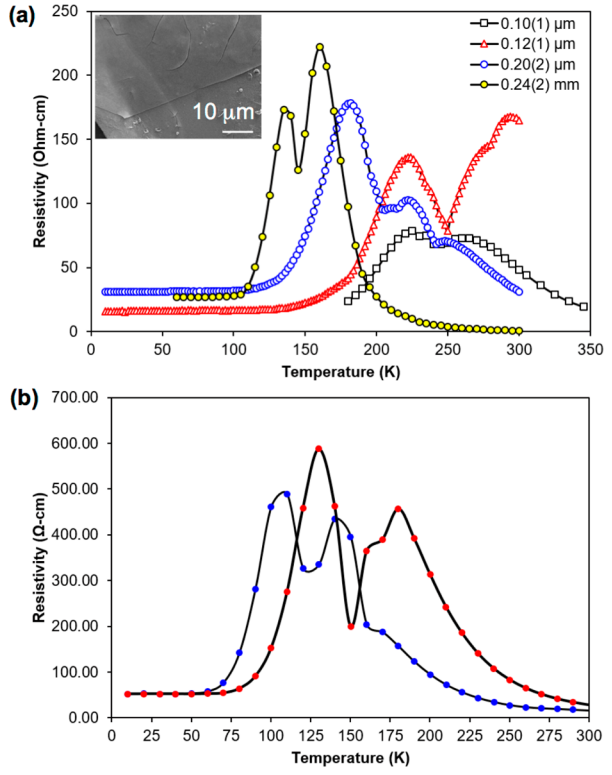

Figure 3. Variable-temperature resistivity data for (a) solid **1** pressed in a pellet of 0.24(2) mm thickness (yellow, scaled down $10^5\times$) and films of **1** with thicknesses of 0.10(1) (black), 0.12(1) (red), and 0.20(2) (blue) μm deposited on glass supports; or (b) films of **1** with thicknesses of 0.5(1) μm before (blue) and after (red) 2 h under vacuum at 90 °C. Inset in panel a: an SEM image of film **1**.

DOI: 10.1021/jacs.7b05742
J. Am. Chem. Soc. 2017, 139, 10863–10867

subsequently seen between 130 and 50 K, suggesting a transition to a metallic phase where scattering of the carriers is dominated by lattice vibrations. The transition is fully reversible, with no signs of hysteresis as illustrated in Figure S7, suggesting it is second order in nature, unlike the metal-to-insulator transitions in materials like VO_2 that are associated with structural deformations.[14] To further confirm the absence of a coherent structural distortion, variable temperature synchrotron powder X-ray diffraction studies were performed between 300 and 100 K. As indicated in Figures S8−10, the only significant change to the diffraction patterns is a slight shift in the [001] reflection from 7.11° (300 K) to 7.15° (100 K), which corresponds to a 0.02 Å contraction of the interlayer spacing or a roughly 1% change.

To explore this transition further, films of **1** were deposited on glass supports with scanning electron microscopy (SEM) images indicating smooth surfaces and good coverage (Figures 3a inset and S11). The thicknesses of the films were determined using atomic force microscopy (AFM) and ranged from 0.1 and 0.2 μm (Figures S12 and 13) with the resistivity being measured in an identical fashion to the pellets described earlier (Figures 3 and S14−18). For films with a thickness of 0.20 μm, the resistivity at 300 K was 31 Ω·cm, corresponding to a conductivity of 3.2×10^{-2} S·cm^{-1}, which is a full order of magnitude higher than the conductivity of the pellet as expected when grain boundaries between the sheet-like particles are reduced. The temperature-dependent resistivity data of the films show a similar semiconductor-to-metal transition (Figure 3a). Interestingly, the transition temperature exhibits a strong correlation with film thickness, with thinner films displaying a higher temperature transition to a metallic state and thicker films remaining semiconducting to lower temperatures (Table S1).

The nanoporous nature of MOFs is well-known to result in a significant amount of solvent being trapped within the channels.[3] To investigate if the presence of trapped solvent has an influence on the transition temperature, the variable temperature resistivity data of a film of 0.5(1) μm thickness was measured before and after 2 h under vacuum at 90 °C (Figures 3b, S19, and 20). These measurements clearly indicate that the films with less solvent display an increase in the metallic transition temperature from 105 to 130 K. XPS studies before and after the conductivity experiments show no significant changes suggesting that the films are not significantly altered by the thermal treatment (Figure S21).

On closer inspection of the transition, there are clearly two closely spaced maxima in the resistivity data. While unusual, this type of transition has been observed in the glassy charge transfer salt κ-(BEDT-TTF)$_2$Cu[N(CN)$_2$]Br (where BEDT-TTF = bis-ethylenedithiotetrathiafulvalene).[15] In this instance, the authors ascribed the unusual temperature dependence to a strong contribution from lattice vibrations at higher temperatures in combination with highly anisotropic changes to the in-plane lattice parameters. Both of these effects are likely at play in **1** as the temperature-dependent synchrotron diffraction data shows a substantially more pronounced change to the interlayer spacing compared to the in-plane distances within the sheets. Considering that the transitions in the resistivity are not reflected in the magnetic susceptibility, they are unlikely to be associated with an in-plane structural distortion, which should alter the coupling between the spins. Furthermore, the removal of solvent from the material would most likely result in a tighter packing of crystallites and more interfacial contact between the sheet-like particles. Thus, our experimental data suggests that changes in the vibrational modes, interlayer spacing and morphological changes (such as contact at the grain boundaries) that interfere with intersheet interactions have the most significant impact on the conductivity of the material.

In order to rationalize these observations in terms of the electronic structure of the framework, DFT calculations were performed (see SI). The calculated band dispersion and density of states (DOS; Figure 4) indicates the compound is actually a

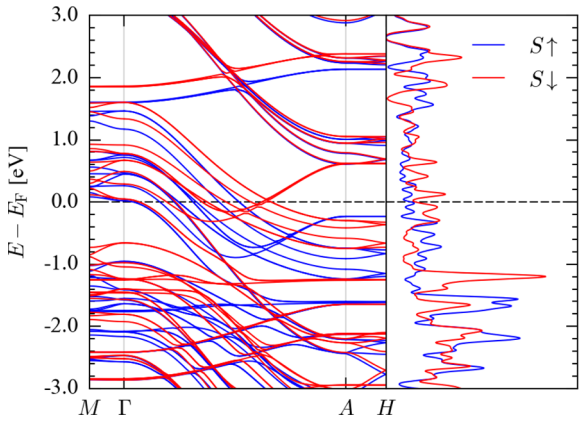

Figure 4. Calculated electronic dispersion and density-of-states curve for **1**.

semimetal, with a small DOS at the Fermi energy (E_F) in both spin channels. There is a large dispersion of ∼2 eV along the Γ-A line in the Brillouin zone, corresponding to the *c*-axis in real space. The smallest calculated carrier effective mass for the metallic bands of 0.29 m$_e$ (see SI) suggests facile transport along this direction, and contrasts with a minimum effective mass of 1.27 m$_e$ along the in-plane directions. The bands making up the metallic states correspond to π-type crystal orbitals centered on the metal ions and ligand S atoms, which explains the large dispersion and suggests that the primary mechanism for conductivity is through conductive pathways along the *c*-axis. This is despite fairly strong covalent bonding between the metal and ligand, as inferred from a Bader-charge analysis (see SI).[16]

To further investigate the stacking mode in **1**, DFT potential energy surface (PES) calculations were performed on a bilayer model with offsets of up to 4 Å along the *a* and *b* axes (Figure 5). These studies show that the fully eclipsed AA structure is the most energetically favored, although a relatively shallow local

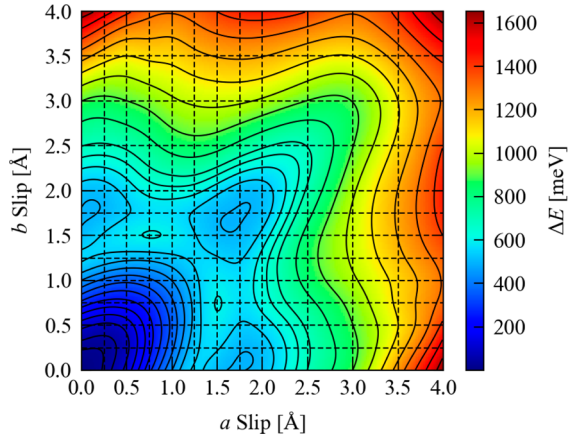

Figure 5. Contour map of the DFT potential energy surface for offsets of alternate layers along the *a* and *b* axes in **1**.

DOI: 10.1021/jacs.7b05742
J. Am. Chem. Soc. 2017, 139, 10863−10867

minimum is present at offsets of ~1.75 Å along one or both axes. Displacements of ±0.25 Å along either or both axes would easily be possible given the thermal energy available at 300 K. These findings also offer some mechanistic insight into the temperature-induced semiconductor-to-metal transition. Thermal expansion along the *c*-direction, or stacking faults leading to misalignment of the layers, were found to introduce a gap in the conduction states (Figures S27–30), which, in combination with a change in the Fermi level, or other factors such as the behavior of the guest molecules in the pore, could play a role in the transition to a narrow-gap semiconductor.

Metallic conductivity has been suggested previously in a nickel benzenehexathiolate framework using first-principles band structure calculations; however, conductivity measurements on a single microflake revealed semiconducting behavior with a small activation energy (E_a) of 26 meV.[7c] The discrepancy was attributed to structural disorder in the sample.[7c] Moreover, DFT calculations performed on $Ni_3(HITP)_2$ framework suggested that the bulk form is metallic, whereas the monolayer form showed a small band gap of 0.25 eV.[7e] The most energetically favored structure for $Ni_3(HITP)_2$ was reported to be an AB slipped-parallel stacking mode wherein one layer was slipped relative to the neighboring one by 1.8 Å along the *a* or *b* vectors.[7a] Additionally, metal substitution was shown by DFT studies to promote or change the electronic properties of these 2D frameworks from semiconducting to metallic.[7e,16,17]

CONCLUSIONS

In summary, we have investigated the temperature-dependent resistivity of a cobalt 2,3,6,7,10,11-triphenylenehexathiolate framework. Variable temperature resistivity studies performed on a pressed-powder pellet indicate a semiconducting phase between 300 and 170 K, followed by a transition to metallic behavior at temperatures below 130 K, which has been unprecedented in MOFs. A similar transition is observed for films, with the transition temperature being highly dependent on the film thickness. Electronic-structure calculations support the experimentally observed complex metallic conductivity, with the highest mobility pathways occurring between the sheets. The temperature-dependence of the resistivity exhibits multiple maxima, which suggests that contributions from stacking faults, local molecular vibrations, and the behavior of solvent molecules in the pores may all be convoluted together to produce a complex mechanism for scattering the charge carriers.

Overall, these results identify the first experimentally observed MOF that exhibits band-like metallic conductivity, and highlights the importance of external factors like guest molecules and film morphology in obtaining highly conductive 2D frameworks. We expect the design principles discovered in these fundamental studies to have a profound impact in understanding the charge transport characteristics of MOFs, leading to new materials with impressive electrical properties.

ASSOCIATED CONTENT

Supporting Information

The Supporting Information is available free of charge on the ACS Publications website at DOI: 10.1021/jacs.7b05742.

Additional procedures and data, and spectroscopic characterization (PDF)

AUTHOR INFORMATION

Corresponding Authors

*smarines@usc.edu
*melot@usc.edu

ORCID

Aron Walsh: 0000-0001-5460-7033
Brent C. Melot: 0000-0002-7078-8206
Smaranda C. Marinescu: 0000-0003-2106-8971

Notes

The authors declare no competing financial interest.

ACKNOWLEDGMENTS

We are grateful to USC and the Women in Science and Engineering for funding, and USC Dornsife for research fellowships to J.W.Y. B.C.M. gratefully acknowledges funding through Office of Naval Research Grant No. N00014-15-1-2411. XPS and SEM data were collected at the Center for Electron Microscopy and Microanalysis (CEMMA), USC. Use of the Advanced Photon Source at Argonne National Laboratory was supported by the U.S. Department of Energy, Office of Science, Office of Basic Energy Sciences, under Contract No. DE-AC02-06CH11357. J.M.S. gratefully acknowledges support from the Engineering and Physical Sciences Research Council (EPSRC) (grant nos. EP/K004956/1 and EP/P007821/1). Calculations were performed on the SiSu facility at the CSC, Finland, via PRACE project no. 13DECI0317/IsoSwitch, and on the Archer facility through the UK Materials Chemistry Consortium, funded by EPSRC grant no. EP/L000202. We also used resources provided by the University of Bath HPC service. We are grateful to John Chen and Sean Culver for assistance with the AFM and BET measurements, respectively.

REFERENCES

(1) (a) Gray, H. B. *Nat. Chem.* **2009**, *1*, 7. (b) Roger, I.; Shipman, M. A.; Symes, M. D. *Nat. Rev. Chem.* **2017**, *1*, 0003. (c) Seh, Z. W.; Kibsgaard, J.; Dickens, C. F.; Chorkendorff, I.; Nørskov, J. K.; Jaramillo, T. F. *Science* **2017**, *355*, eaad4998.

(2) McKone, J. R.; Marinescu, S. C.; Brunschwig, B. S.; Winkler, J. R.; Gray, H. B. *Chem. Sci.* **2014**, *5*, 865.

(3) O'Keeffe, M.; Yaghi, O. M. *Chem. Rev.* **2012**, *112*, 675.

(4) (a) Hendon, C. H.; Tiana, D.; Walsh, A. *Phys. Chem. Chem. Phys.* **2012**, *14*, 13120. (b) Talin, A. A.; Centrone, A.; Ford, A. C.; Foster, M. E.; Stavila, V.; Haney, P.; Kinney, R. A.; Szalai, V.; El Gabaly, F.; Yoon, H. P.; Léonard, F.; Allendorf, M. D. *Science* **2014**, *343*, 66. (c) Leong, C. F.; Usov, P. M.; D'Alessandro, D. M. *MRS Bull.* **2016**, *41*, 858. (d) Dolgopolova, E. A.; Brandt, A. J.; Ejegbavwo, O. A.; Duke, A. S.; Maddumapatabandi, T. D.; Galhenage, R. P.; Larson, B. W.; Reid, O. G.; Ammal, S. C.; Heyden, A.; Chandrashekhar, M.; Stavila, V.; Chen, D. A.; Shustova, N. B. *J. Am. Chem. Soc.* **2017**, *139*, 5201. (e) Stassen, I.; Burtch, N.; Talin, A.; Falcaro, P.; Allendorf, M.; Ameloot, R. *Chem. Soc. Rev.* **2017**, *46*, 3185.

(5) (a) Cote, A. P.; Benin, A. I.; Ockwig, N. W.; O'Keeffe, M.; Matzger, A. J.; Yaghi, O. M. *Science* **2005**, *310*, 1166. (b) Makiura, R.; Motoyama, S.; Umemura, Y.; Yamanaka, H.; Sakata, O.; Kitagawa, H. *Nat. Mater.* **2010**, *9*, 565. (c) Colson, J. W.; Woll, A. R.; Mukherjee, A.; Levendorf, M. P.; Spitler, E. L.; Shields, V. B.; Spencer, M. G.; Park, J.; Dichtel, W. R. *Science* **2011**, *332*, 228. (d) Kambe, T.; Sakamoto, R.; Hoshiko, K.; Takada, K.; Miyachi, M.; Ryu, J. H.; Sasaki, S.; Kim, J.; Nakazato, K.; Takata, M.; Nishihara, H. *J. Am. Chem. Soc.* **2013**, *135*, 2462. (e) So, M. C.; Jin, S.; Son, H.-J.; Wiederrecht, G. P.; Farha, O. K.; Hupp, J. T. *J. Am. Chem. Soc.* **2013**, *135*, 15698.

(6) (a) Kobayashi, Y.; Jacobs, B.; Allendorf, M. D.; Long, J. R. *Chem. Mater.* **2010**, *22*, 4120. (b) Wan, S.; G andara, F.; Asano, A.; Furukawa, H.; Saeki, A.; Dey, S. K.; Liao, L.; Ambrogio, M. W.; Botros, Y. Y.; Duan,

DOI: 10.1021/jacs.7b05742
J. Am. Chem. Soc. 2017, 139, 10863–10867

X.; Seki, S.; Stoddart, J. F.; Yaghi, O. M. *Chem. Mater.* **2011**, *23*, 4094. (c) Hmadeh, M.; Lu, Z.; Liu, Z.; Gandara, F.; Furukawa, H.; Wan, S.; Augustyn, V.; Chang, R.; Liao, L.; Zhou, F.; Perre, E.; Ozolins, V.; Suenaga, K.; Duan, X.; Dunn, B.; Yamamto, Y.; Terasaki, O.; Yaghi, O. M. *Chem. Mater.* **2012**, *24*, 3511. (d) Cai, S.-L.; Zhang, Y.-B.; Pun, A. B.; He, H.; Yang, J.; Toma, F. M.; Sharp, I. D.; Yaghi, O. M.; Fan, J.; Zheng, S.-R.; Zhang, W.-G.; Liu, Y. *Chem. Sci.* **2014**, *5*, 4693. (e) Sun, L.; Campbell, M. G.; Dincă, M. *Angew. Chem., Int. Ed.* **2016**, *55*, 3566. (f) Cui, J.; Xu, Z. *Chem. Commun.* **2014**, *50*, 3986. (g) Darago, L. E.; Aubrey, M. L.; Yu, C. J.; Gonzalez, M. I.; Long, J. R. *J. Am. Chem. Soc.* **2015**, *137*, 15703.

(7) (a) Sheberla, D.; Sun, L.; Blood-Forsythe, M. A.; Er, S.; Wade, C. R.; Brozek, C. K.; Aspuru-Guzik, A.; Dincă, M. *J. Am. Chem. Soc.* **2014**, *136*, 8859. (b) Campbell, M. G.; Sheberla, D.; Liu, S.; Swager, T. M.; Dincă, M. *Angew. Chem., Int. Ed.* **2015**, *54*, 4349. (c) Kambe, T.; Sakamoto, R.; Kusamoto, T.; Pal, T.; Fukui, N.; Hoshiko, K.; Shimojima, T.; Wang, Z.; Hirahara, T.; Ishizaka, K.; Hasegawa, S.; Liu, F.; Nishihara, H. *J. Am. Chem. Soc.* **2014**, *136*, 14357. (d) Huang, X.; Sheng, P.; Tu, Z.; Zhang, F.; Wang, J.; Geng, H.; Zou, Y.; Di, C.; Yi, Y.; Sun, Y.; Xu, W.; Zhu, D. *Nat. Commun.* **2015**, *6*, 7408. (e) Foster, M. E.; Sohlberg, K.; Spataru, C. D.; Allendorf, M. D. *J. Phys. Chem. C* **2016**, *120*, 15001.

(8) Clough, A. J.; Yoo, J. W.; Mecklenburg, M. H.; Marinescu, S. C. *J. Am. Chem. Soc.* **2015**, *137*, 118.

(9) (a) Lin, S.; Diercks, C. S.; Zhang, T.-B.; Kornienko, N.; Nichols, E. M.; Zhao, Y.; Paris, A. R.; Kim, D.; Yang, P.; Yaghi, O. M.; Chang, C. J. *Science* **2015**, *349*, 1208. (b) Hod, I.; Sampson, M. D.; Deria, P.; Kubiak, C. P.; Farha, O. K.; Hupp, J. T. *ACS Catal.* **2015**, *5*, 6302. (c) Miner, E. M.; Fukushima, T.; Sheberla, D.; Sun, L.; Surendranath, Y.; Dincă, M. *Nat. Commun.* **2016**, *7*, 10942. (d) Dong, R.; Pfeffermann, M.; Liang, H.; Zheng, Z.; Zhu, X.; Zhang, J.; Feng, X. *Angew. Chem., Int. Ed.* **2015**, *54*, 12058. (e) Dong, R.; Zheng, Z.; Tranca, D. C.; Zhang, J.; Chandrasekhar, N.; Liu, S.; Zhuang, X.; Seifert, G.; Feng, X. *Chem. - Eur. J.* **2017**, *23*, 2255.

(10) (a) Cairns, A. B.; Goodwin, A. L. *Chem. Soc. Rev.* **2013**, *42*, 4881. (b) Ramesh, T. N.; Jayashree, R. S.; Kamath, P. V. *Clays Clay Miner.* **2003**, *51*, 570.

(11) Orchard, A. F. *Magnetochemistry*; Oxford University Press, 2003.

(12) (a) Ray, K.; Begum, A.; Weyhermüller, T.; Piligkos, S.; van Slageren, J.; Neese, F.; Wieghardt, K. *J. Am. Chem. Soc.* **2005**, *127*, 4403. (b) Sproules, S.; Wieghardt, K. *Coord. Chem. Rev.* **2011**, *255*, 837.

(13) Smith, C. E.; Odoh, S. O.; Ghosh, S.; Gagliardi, L.; Cramer, C. J.; Frisbie, C. D. *J. Am. Chem. Soc.* **2015**, *137*, 15732.

(14) (a) Corr, S. A.; Shoemaker, D. P.; Melot, B. C.; Seshadri, R. *Phys. Rev. Lett.* **2010**, *105*, 056404. (b) Goodenough, J. B. *J. Solid State Chem.* **1971**, *3*, 490. (c) Park, J.; Oh, I. H.; Lee, E.; Lee, K. W.; Lee, C. E.; Song, K.; Kim, Y.-J. *Appl. Phys. Lett.* **2007**, *91*, 153112.

(15) (a) Hartmann, B.; Müller, J.; Sasaki, T. *Phys. Rev. B: Condens. Matter Mater. Phys.* **2014**, *90*, 195150. (b) Kato, R. *Chem. Rev.* **2004**, *104*, 5319.

(16) Shojaei, F.; Hahn, J. R.; Kang, H. S. *Chem. Mater.* **2014**, *26*, 2967.

(17) (a) Chen, S.; Dai, J.; Zeng, X. C. *Phys. Chem. Chem. Phys.* **2015**, *17*, 5954. (b) Chakravarty, C.; Mandal, B.; Sarkar, P. *J. Phys. Chem. C* **2016**, *120*, 28307. (c) Sun, L.; Hendon, C. H.; Park, S. S.; Tulchinsky, Y.; Wan, R.; Wang, F.; Walsh, A.; Dincă, M. *Chem. Sci.* **2017**, *8*, 4450.

DOI: 10.1021/jacs.7b05742
J. Am. Chem. Soc. 2017, 139, 10863−10867